The Significance of Austenite/Ferrite/Martensite Ratio on Governing Impact Toughness of Fe-0.2C-6Mn-1.5Al Medium-Mn Transformation-Induced Plasticity Steel Studied by a Novel Heat Treatment

Zhichao Li, Yanjie Mou, Xinjing Li, Devesh Misra, Lianfang He, and Huiping Li

In this paper, the scientific challenges associated with obtaining high impact toughness in the medium-Mn TRIP steel, Fe-0.2C-6Mn-1.5Al, have been explored. This was enabled by a novel and effective heat treatment involving the combination of intercritical hardening and tempering to obtain high impact toughness. Electron microscopy and x-ray diffraction studies clearly underscored absence of TRIP effect in Fe-0.2C-6Mn-1.5Al medium manganese steel during impact and the volume fraction of austenite played a determining role in governing impact toughness. The highest impact toughness of 180.17 J/cm^2 was obtained when the steel was subjected to intercritical hardening temperature of 630 °C and low tempering temperature of 200 °C. The presence of martensite in the microstructure reduced the impact toughness on quenching from 670 to 700 °C. When the quenching temperature was increased to 750 °C, the impact toughness of steel was slightly increased, which is ascribed to the supersaturated carbon in martensite that precipitated as carbides. The fracture mode was ductile after intercritical hardening in the temperature range of 600-700 °C.

1. Introduction

With the continuous increase in car ownership and energy exhaustion, there are new requirements for energy saving and emission reduction of cars, besides safety performance of automobiles. There is need for next generation of high strength steels with low cost. In this regard, there is increased focus on medium manganese steels, as third generation of automobile steels (Ref 1-5). Impact properties of medium-Mn steel are an important mechanical property index of automobile steel. It refers to the ability of material to absorb plastic deformation and fracture work under impact load, reflecting the tiny defects and impact resistance of material. Impact toughness reflects the resistance of metal materials to external impact load.

In recent years, the relationship between mechanical properties and microstructure of medium manganese steel has been widely studied. A large number of studies focused on heat treatment of medium manganese steels (Ref 6-8). Particularly,

with respect to the relationship between mechanical properties and austenite content in medium manganese steels, researchers found that the TRIP steel with a high volume fraction of austenite exhibited best combination of ultimate tensile strength and ductility (Ref 9-11). But studies on the effect of austenite, martensite and ferrite on impact properties of medium manganese steels are rare. Yamanaka et al. (Ref 12) studied the relationship between martensite and impact properties of medium manganese steels, but ignored the effect of austenite and ferrite.

Based on the above, the objective here is to explore ferrite/martensite ratio in governing impact toughness. To accomplish the objective, a novel heat treatment was designed that involved intercritical annealing in the two-phase temperature range of 600-750 °C of Fe-0.2C-6Mn-1.5Al steel, followed by quenching to room temperature and tempering at 200 °C.

2. Experimental Procedure

The chemical composition of the present steel was Fe-0.20C-6.16Mn-1.62Al (wt.%). Forty kilograms of cast ingots (200 mm diameter cylinder) was refined using a vacuum melting furnace and then forged into a slab with a cross-section dimension of section size 100 mm × 30 mm. Subsequently, the rods were hot-rolled into about 4.0 mm in thickness after reheating to 1200 °C for 2 h. The amount of reduction is 86.7% during hot rolling. A schematic of the rolling process is shown in Fig. 1.

For medium-Mn steels mentioned, the traditional heat treatment requires a long intercritical annealing time, and it is difficult to use for the experimental steel studied here (Ref 13-
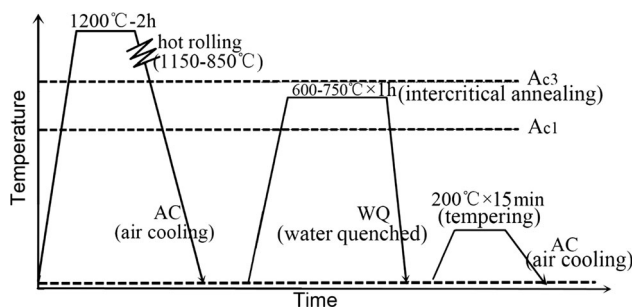
Zhichao Li, Yanjie Mou, Xinjing Li, Lianfang He, and **Huiping Li**, School of Materials Science and Engineering, Shandong University of Science and Technology, Qingdao 266590 Shandong, China; and **Devesh Misra**, Laboratory for Excellence in Advanced Steel Research, Department of Metallurgical, Materials and Biomedical Engineering, University of Texas at El Paso, El Paso, TX 79968. Contact e-mails: lizhichao198918@163.com, dmisra2@utep.edu, and lihuiping99@163.com.

18). Thus, an effective and novel heat treatment with two-stage process was adopted (as shown in Fig. 1): (1) First process, intercritical hardening, steels were soaked in the intercritical temperature region for 1 h and then quenched in water. (2) Second process, tempering, the steels after quenching were tempered at low temperature 200 °C for 15 min and then immediately cooled in air to room temperature.
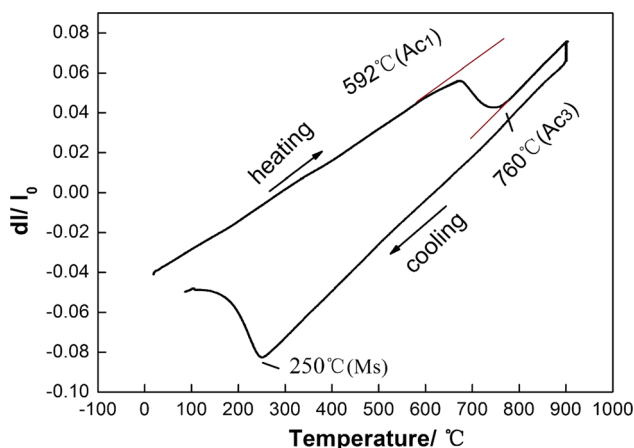
The dilatometric plot of the experimental steel is presented in Fig. 2. After thermal expansion during heating stage (30-900 °C) at the rate of 20 °C/s, the sample was held at 900 °C for 3 min. The intercritical temperature range of the experimental steel was 592-760 °C, as marked in Fig. 2.

Five temperatures, namely 600, 630, 670, 700, and 750 °C, were selected in the two-phase region and soaked for 1 h and then quenched to room temperature, followed by tempering at 200 °C for 20 min. Charpy v-notch impact specimens were made from the heat-treated plates and impact tested using JB-300B semiautomatic impact tester at room temperature.

The microstructure was characterized by field-emission scanning electron microscopy (SEM), nanoindentation (Keysight G200XT nanoindenter system: Lateral displacement resolution: 150 nm; Background noise of lateral displacement: 0.5 nm), electron backscatter diffraction (EBSD), field-emission transmission electron microscopy (TEM) and x-ray diffraction (XRD). EBSD surface specimens were made by electropolishing. The electropolishing solution is 85% anhydrous ethanol + 15% perchloric acid, the polishing voltage is 20 V, and the time is 30 s. In order to obtain thin area for TEM observation, the specimen with diameter of 3 mm was electro-

plated and thinned. The electrolyte is 20% perchloric acid + 80% anhydrous ethanol, and a direct current of 30 V, 15 mA is applied at both ends of the electrode. In the process of double spraying, liquid nitrogen should be used for cooling, and the temperature of electrolyte should always be lower than − 25 °C. The volume fraction of austenite was determined by x-ray diffraction (XRD) with CuK$_\alpha$ radiation using the direct comparison method (Ref 19). The volume fraction of austenite was measured using the integrated intensities of $(220)_\gamma$ and $(311)_\gamma$ peaks of austenite and $(200)_\alpha$ and $(211)_\alpha$ peaks of ferrite. The volume fraction of austenite, V_A, was calculated by Eq. (1) (Ref 20):

$$V_A = \frac{\frac{1}{N}\sum_{i=1}^{N}\frac{I_\gamma,i}{R_\gamma,i}}{\frac{1}{N}\sum_{i=1}^{N}\frac{I_\gamma,i}{R_\gamma,i} + \frac{1}{M}\sum_{i=1}^{M}\frac{I_\alpha,i}{R_\alpha,i}} \quad \text{(Eq 1)}$$
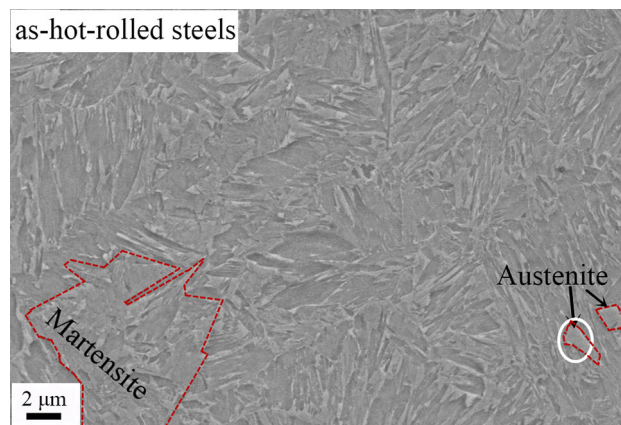
where I_α and I_γ are integrated intensity values of ferrite α-phase and austenite, respectively. M and N are the numbers of ferrite peaks and austenite peaks, respectively. R_α and R_γ are the standardization constant of ferrite and austenite, respectively. $R_{\gamma, (220)} = 1.796$ m^{-1}, $R_{\gamma, (311)} = 2.282$ m^{-1}, $R_{\alpha, (211)} = 2.932$ m^{-1}, and $R_{\alpha, (200)} = 1.269$ m^{-1}.
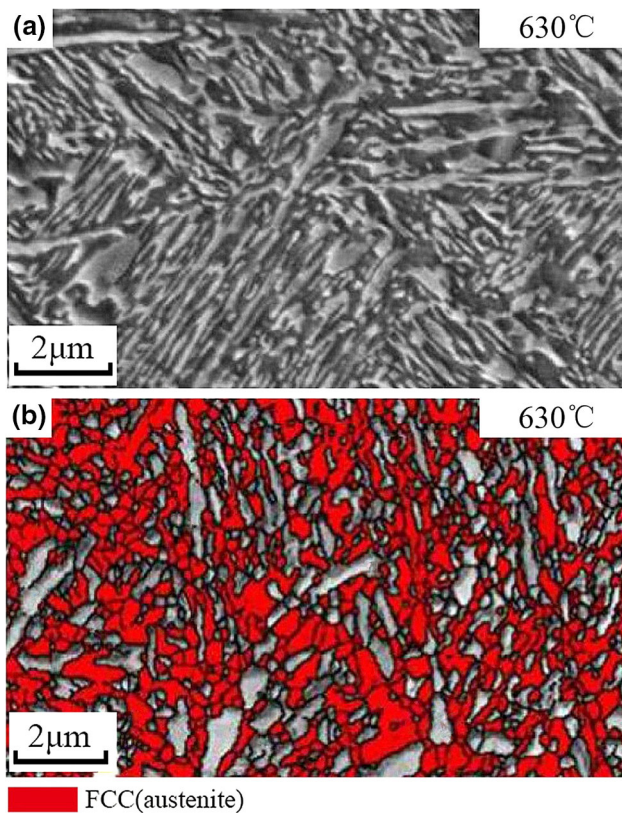
3. Results and Discussion

3.1 Microstructure Evolution

Figure 3 is a representative SEM micrograph of as-hot-rolled steel. The microstructural constituents consisted of martensite and small amount of austenite. During rolling, most of austenite transformed into martensite. Due to the volume expansion of martensite, the grain boundary between martensite and retained austenite was not clear, and ferrite was not easy to be identified due to extrusion. During intercritical treatment, martensite reverted to austenite.

From the representative SEM micrograph in Fig. 4(a), it can be seen that the microstructure of hot-rolled steel on quenching from 630 °C and tempering at 200 °C mainly consisted of lath-type grains. In order to characterize these grains, EBSD studies were carried out, as shown in Fig. 4(b). Some grains were identified to have FCC structure, i.e., reversed austenite, but there was also some BCC phase, i.e., ferrite.

Fig. 1 Schematic diagram of hot rolling and heat treatment schedule for steels using an effective and simple two-stage heat treatment process

Fig. 2 Dilatometric plot for the experimental steel

Fig. 3 SEM micrographs of as-hot-rolled steel

Fig. 4 Microstructure of hot-rolled steel on quenching from the intercritical annealing temperature of 630 °C and tempering at 200 °C: (a) representative SEM micrograph, (b) EBSD characterization showing the morphology and distribution of reversed austenite grains (red) overlaid on the image quality maps (Color figure online)

SEM micrographs of intercritical hardened and tempered steels are shown in Fig. 5. The microstructure of steels was comprised of intercritical ferrite (α-ferrite), martensite, and retained austenite. The amount of stripe-like ferrite decreased with the increase in temperature, while the austenite with thin lath gradually widened with the increase in temperature. As shown in marked rectangle in Fig. 5(c), in the parent austenite matrix, the thin lathy martensite was dispersed, which can be broadly divided into thin layer-type and granular on quenching from 670 °C for the experimental steel.

According to the Fe–C phase diagram, with the increase in intercritical temperature, ferrite content is expected to decrease, and the amount of austenite to increase, and growth of austenite grains occurs. With the increase in austenite grain size, the stability of austenite decreases (Ref 21, 22). During quenching, more austenite is transformed to martensite. Thus, with the increase in annealing temperature, the amount of martensite increased on quenching. Austenite in the experimental steels had a high fraction on quenching in the temperature range of 600-630 °C, but when they were heat-treated at 670 °C, the amount of austenite decreased markedly because of extensive martensitic transformation. When the quenching temperature was increased from 670 to 750 °C, the amount of martensite increased gradually because of decrease of austenite stability. Moreover, nanoindentation (Keysight G200XT nanoindenter system) test was performed for the 0.20C-8.65Mn-4.12Al-Fe sample after quenching from 750 °C and tempering at 200 °C

(Fig. 6). This showed difference in hardness between austenite, α-ferrite, and martensite.

The microstructure evolution of experimental steels on quenching from 630 to 670 °C, respectively, was characterized by TEM and is presented in Fig. 7. In the steel quenched from 630 °C, the microstructure showed lamellar structure with alternate bright and dark lath, which were identified as ferrite lath and austenite lath, as shown by the inserted selected area diffraction (SAD) in Fig. 7(a). The martensite structure of steel quenched from 670 °C was characterized by TEM (Fig. 7b). The microstructure was nearly martensite with retained austenite (dark lath) and ferrite (bright-lath).

Figure 8 shows XRD pattern and measured volume fraction of austenite in steels on quenching from different intercritical temperatures. The volume fraction of retained austenite increased from 36.2 to 57.1 vol.% when the quenching temperature was increased from 600 to 630 °C, followed by a significant decrease to 41.9% on quenching from 670 °C. Finally, the volume fraction of retained austenite decreased to 12.3 vol.% when the quenching temperature was increased to 750 °C.

Figure 9 shows a schematic representation of ferrite, retained austenite and martensite volume fraction in the experimental steel intercritically hardened at different temperatures. The accurate volume fraction of austenite can be measured by XRD. But the fraction of ferrite and the martensite is not the actual measurements, it is only a schematic diagram showing the trend of change in volume fraction of ferrite and martensite phases. According to Fe–C phase diagram, with the increase in annealing temperature, the amount of ferrite decreases, the amount of austenite increases, and the austenite grain grows. With the increase in austenite grain size, the stability of austenite decreases. During quenching, more austenite transforms into martensite. Thus, with the increase in annealing temperature from 600 to 630 °C, the volume fraction of austenite was increased and the ferrite volume fraction was decreased. Moreover, on increasing the temperature, the retained austenite grain size increases, which leads to a decrease in stability of austenite. The higher the intercritical hardening temperature, the more amount of austenite is transformed to martensite on quenching from 670 °C and is the reason for decrease in the volume fraction of austenite.

3.2 The Critical Factors Governing Impact Toughness

The variation in impact toughness for steels on quenching from different intercritical temperatures is presented in Fig. 10. At least five samples were tested for each experimental condition. As shown in Fig. 10, the impact toughness of hot-rolled experimental steels was increased with the increase in temperature, with a maximum value of 180.17 J/cm^2 for 630 °C, followed by a decrease to 81.25 J/cm^2 at 700 °C, and again increased to 103.12 J/cm^2 for 750 °C.
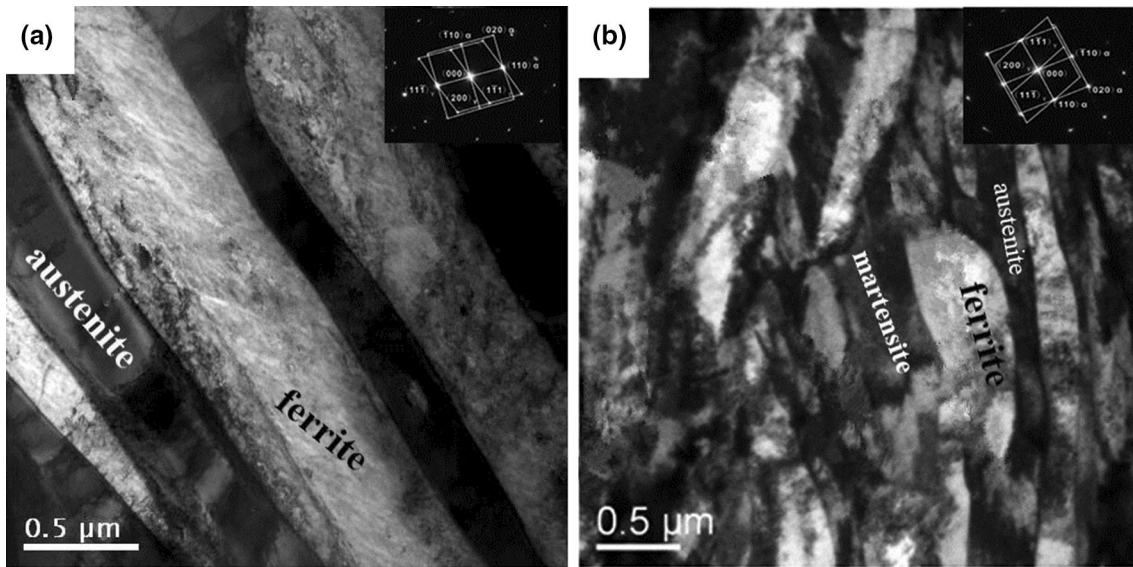
The volume fraction of austenite in experimental steel heat-treated at different temperatures and fractured samples was measured by XRD. Figure 11 shows the volume fraction of austenite in samples before impact test and after impact fracture. Comparing samples before the impact test, the volume fraction of austenite in the samples after impact fracture showed an insignificant change. Thus, it can be inferred that TRIP effect did not occur during impact test. According to the results of high-speed tensile test (Ref 23, 24), the volume fraction of transformed retained austenite decreased obviously with
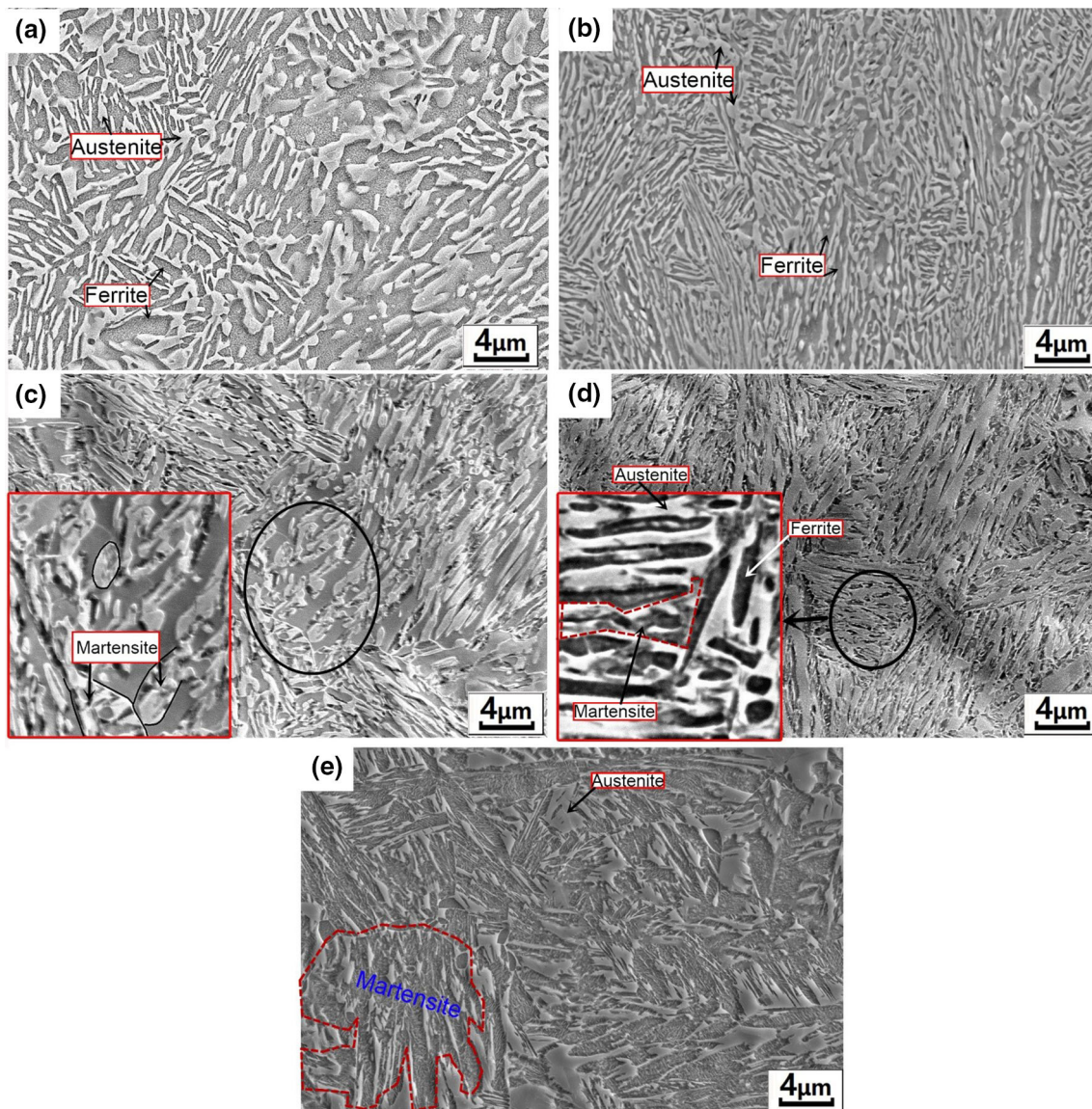
Fig. 5 SEM micrographs of hot-rolled steels on quenching from different intercritical temperatures. (a) 600 °C, (b) 630 °C, (c) 670 °C, (d) 700 °C and (e) 750 °C
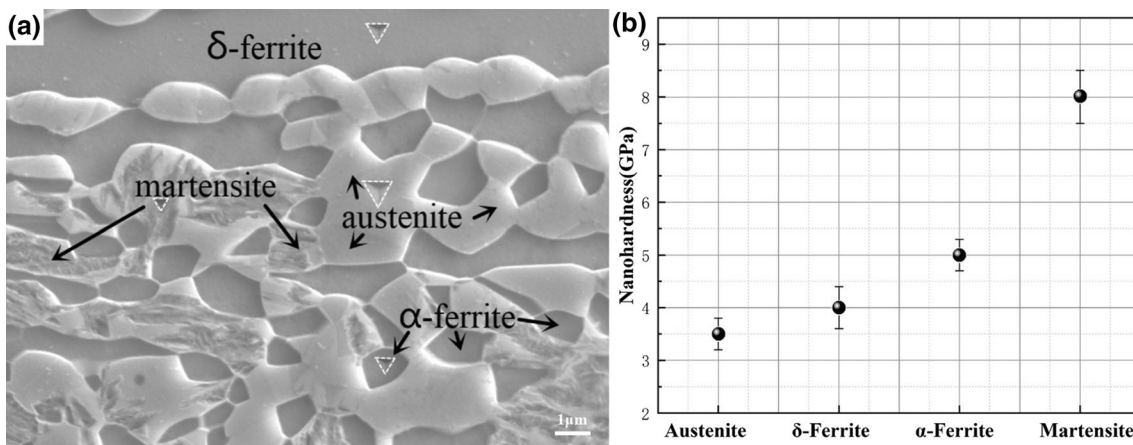

Fig. 6 (a) A SEM image showing the indentation impressions on austenite grains, δ-ferrite grains, α-ferrite grains, and martensite grains in hot-rolled 0.20C-8.65Mn-4.12Al-Fe steels after quenching from intercritical annealing temperature of 750 °C and tempering from 200 °C. (b) The nanohardness values of different phase grains. Each error bar represents a standard deviation

Fig. 7 TEM microstructure evolution of hot-rolled steel after quenching from (a) 630 °C and (b) 670 °C
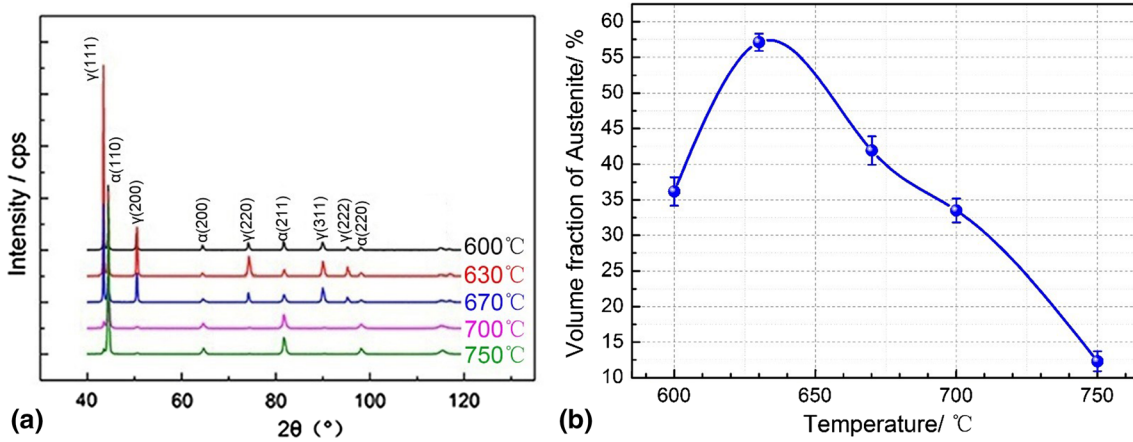
**Fig. 8** XRD patterns and measured austenite fractions of steels heat-treated at different temperatures: (a) XRD patterns for steels and (b) measured austenite fractions
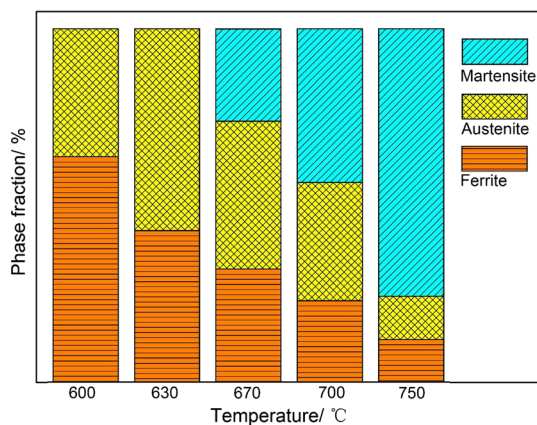
Fig. 9 Schematic diagram of the volume fraction of ferrite, austenite and martensite in steels heat-treated at different temperatures
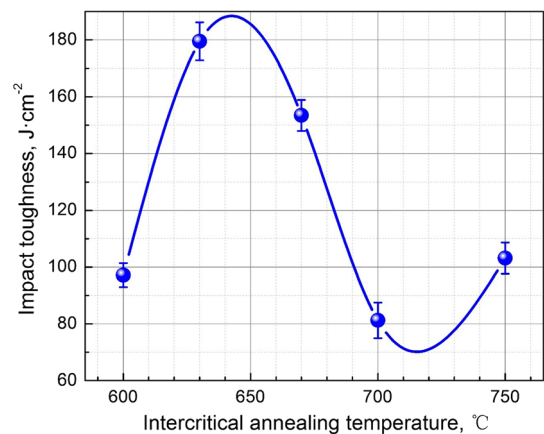
Fig. 10 The variation of impact toughness as a function of intercritical annealing temperature
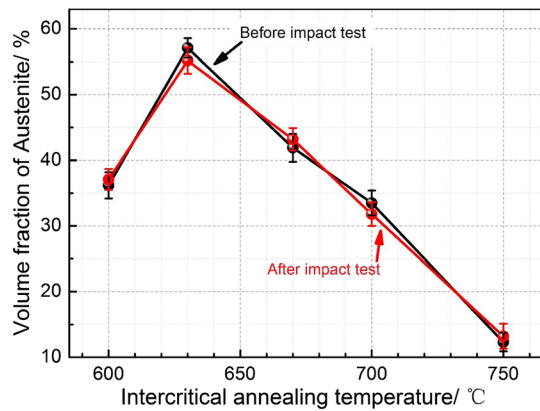
Fig. 11 Volume % austenite fraction in experimental steel heat-treated at different temperatures and fractured samples

increasing strain rate due to the adiabatic temperature rise under high strain rate. In the impact test, austenite did not transform into martensite because of high strain rate. Thus, the improvement in impact toughness is not related to TRIP effect.

In austenitic steels, the increase in impact toughness is mainly related to austenite content (Ref 25-28). As shown in Fig. 6, the hardness of austenite was lowest compared with BCC ferrite, while FCC austenite has stronger deformation ability. We envisage that austenite can reduce stress concentration during impact and increase resistance to deformation, with consequent increase in impact toughness of experimental steel. According to Fig. 8 and 10, when the intercritical quenching temperature was increased from 600 to 630 °C, the volume fraction of austenite increased from 36.2 to 57.1 vol.%, and the impact toughness increased from 97.19 to 180.17 J/cm^2. When the temperature of quench was low, the amount of retained austenite was low and the impact toughness was reduced. When the temperature of quenching increased to 630 °C, the amount of retained austenite increased and impact toughness was enhanced. Interestingly, the impact toughness of experimental steel increased gradually under the effect of increase of retained austenite content. It is concluded that the amount of austenite had a dominant effect on impact toughness.

When the temperature of quench was increased to 670 °C, the grain size of austenite increases and the stability of austenite is reduced, such that austenite transforms to martensite on quenching from 670 °C. The presence of martensite in the microstructure results in volume expansion, stress concentration and high internal stress. Therefore, it is easy to produce cracks during impact, reduce resistance to deformation, and reduce impact toughness of experimental steel. When the quenching temperature was increased from 630 to 670 °C, the impact toughness decreased from 180.17 to 153.43 J/cm^2.

Figure 12 is the TEM micrograph of experimental steel quenched from 750 °C and tempered at 200 °C. It can be seen that on quenching from the intercritical annealed temperature of 750 °C and tempering, the supersaturated carbon in martensite precipitated as carbides on tempering at 200 °C. The precipitation of carbides reduces lattice distortion and internal stress. With the increase in quenching temperature, the matrix softens and absorbs more energy during impact. Moreover, the presence of precipitates will change the direction of crack growth and the stress–strain state ahead of crack. This improves the impact toughness of experimental steel. When the quench-
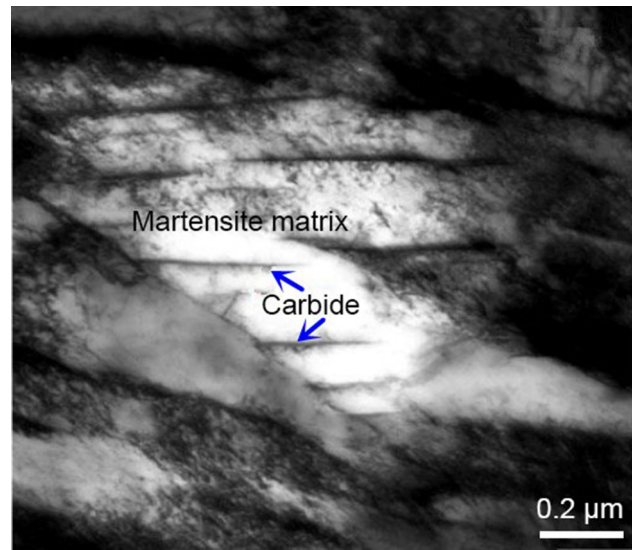
Fig. 12 TEM micrograph of experimental steel quenched from the intercritical annealing temperature of 750 °C and tempered at 200 °C

ing temperature was increased from 700 to 750 °C, the impact toughness increased from 81.25 to 103.12 J/cm^2.
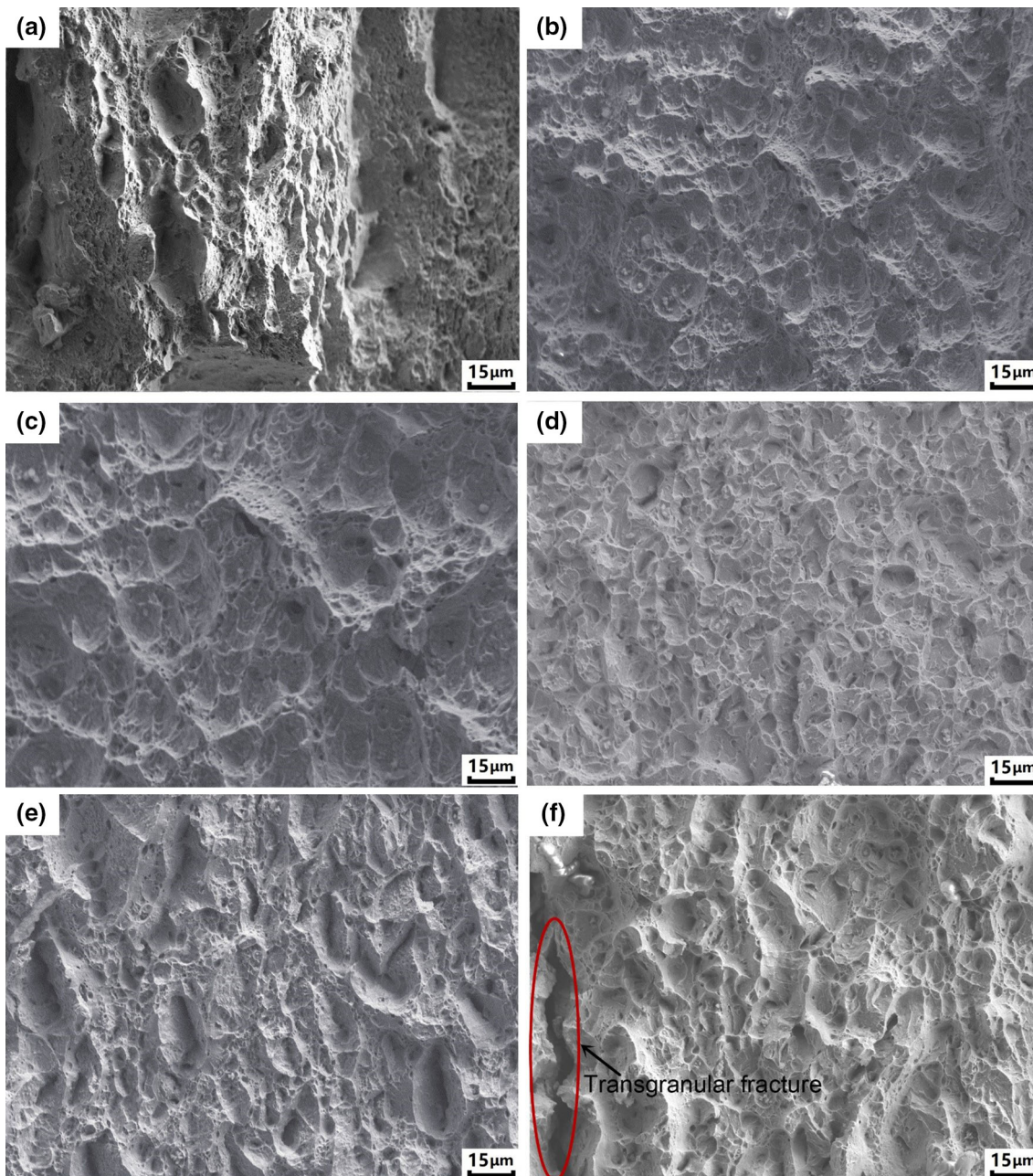
3.3 Fractography

The fracture surface of hot-rolled steels on quenching from different intercritical temperatures was observed using electron probe micro-analyzer (EPMA) to study the fracture mode (Fig. 13). The fracture surface of as-hot-rolled steel without heat treatment is presented in Fig. 13(a). It is clear that the fracture mode was predominantly intergranular and the representative of cleavage brittle fracture were present. As shown in Fig. 13(b), when the quenching temperature was 600 °C, dimples were present on the fracture surface, indicative of ductile fracture. Ductility is related to distribution, depth, number density and size of dimples (Ref 17, 29-31). When the quenching temperature was increased from 600 to 630 °C, the number and size of dimples in the fracture surface were increased, corresponding to the increasing impact toughness. When the quenching temperature was increased to 670 °C, the dimple size gradually decreased, corresponding to the decrease in impact toughness. The fracture surface of steel on quenching from 750 °C is presented in Fig. 13(f). It can be seen that the fracture was ductile and transgranular fracture cracks were also observed. Combining impact toughness data and fracture surface analysis, it can be concluded that the larger the number and size of dimples, the greater is the impact toughness.

4. Conclusions

Different microstructures were obtained in Fe-0.2C-6Mn-1.5Al medium manganese TRIP steel through intercritical annealing and tempering. Combining microstructure evolution, impact toughness and fracture morphology, the following are the conclusions.

1. During the impact process, there was absence of TRIP effect in Fe-0.2C-6Mn-1.5Al medium manganese steel.

Fig. 13 Fractographs of hot-rolled steel (a) and after quenching from different intercritical annealing temperatures. (b) 600 °C, (c) 630 °C, (d) 670 °C, (e) 700 °C, (f) 750 °C

At high strain rate, experienced during the impact test, austenite did not transform to martensite.

2. On quenching from the intercritical annealing temperature range of 600-630 °C and tempering at 200 °C, the content of austenite increased with the increase of intercritical annealing temperature. The effect of austenite content on impact toughness was dominant. Thus, with the increase in intercritical annealing temperature from 600 to 630 °C, the impact toughness was increased from 97.19 to 180.17 J/cm^2.

3. When the intercritical annealing temperature was increased from 630 up to 700 °C, the presence of martensite in the microstructure reduced the impact toughness of experimental steel from 180.17 to 81.25 J/cm^2.

4. The impact toughness was marginally improved for 750 °C, which is ascribed to the fact that the supersaturated carbon in martensite precipitated as carbide.

5. The impact fracture mode of experimental as-hot-rolled steel without heat treatment was brittle cleavage fracture, while it was ductile fracture after annealing in the intercritical temperature range and tempering. The larger the number and size of dimples in the fracture, the higher was the impact toughness of the corresponding experimental steel.

Data Availability

The raw/processed data required to reproduce these findings cannot be shared at this time as the data also forms part of an ongoing study.

References

1. S. Lee, S.J. Lee, and B.C. De Cooman, Austenite Stability of Ultrafine-Grained Transformation-Induced Plasticity Steel with Mn Partitioning, *Scr. Mater.*, 2011, **65**, p 225–228

2. J. Shi, X.J. Sun, M.Q. Wang, W.J. Hui, H. Dong, and W.Q. Cao, Enhanced Work-Hardening Behaviors and Mechanical Properties in Ultrafine-Grained Steels with Large-Fractioned Metastable Austenite, *Scr. Mater.*, 2010, **63**, p 815–818

3. N. Nakada, K. Mizutani, T. Tsuchiyama, and S. Takaki, Difference in Transformation Behavior Between Ferrite and Austenite Formations in Medium Manganese Steel, *Acta Mater.*, 2014, **65**, p 251–258

4. S. Lee, S.J. Lee, S.S. Kumar, K. Lee, and B.C. De Cooman, Localized Deformation in Multiphase Ultra-Fine-Grained 6 Pct Mn Transformation-Induced Plasticity Steel, *Metall. Mater. Trans. A*, 2011, **42A**, p 3638–3651

5. Z.C. Li, R.D.K. Misra, H. Ding, H.P. Li, and Z.H. Cai, The Significant Impact of Pre-strain on the Structure-Mechanical Properties Relationship in Cold-Rolled Medium Manganese TRIP steel, *Mater. Sci. Eng., A*, 2018, **712**, p 206–213

6. R.H. Cao, J.H. Liang, F. Li, C. Li, and Z.Z. Zhao, Intercritical Annealing Processing and a New Type of Quenching and Partitioning Processing, Actualized by Combining Intercritical Quenching and Tempering, for Medium Manganese Lightweight Steel, *Steel Res. Int.*, 2019, **1900335**, p 1–7

7. N. Yan, H.S. Di, R.D.K. Misra, H.Q. Huang, and Y.L. Li, Enhancing Austenite Stability in a New Medium-Mn Steel by Combining Deep Cryogenic Treatment and Intercritical Annealing: An Experimental and Theoretical Study, *Mater. Sci. Eng., A*, 2019, **753**, p 11–21

8. T. Tsuchiyama, T. Inoue, J. Tobata, D. Akama, and S. Takaki, Microstructure and Mechanical Properties of a Medium Manganese Steel Treated with Interrupted Quenching and Intercritical annealing, *Scr. Mater.*, 2016, **12**, p 236–239

9. Z.C. Li, X.T. Zhang, Y.J. Mou, R.D.K. Misra, L.F. He, and H.P. Li, The Impact of Intercritical Annealing in Conjunction with Warm Deformation Process on Microstructure, Mechanical Properties and TRIP Effect in Medium-Mn TRIP Steels, *Mater. Sci. Eng., A*, 2019, **746**, p 363–371

10. X. Qi, L.X. Du, J. Hu, and R.D.K. Misra, Effect of Austenite Stability on Toughness, Ductility, and Work-Hardening of Medium-Mn Steel, *Mater. Sci. Technol.*, 2019, **35**, p 2134–2142

11. G. Su, X. Gao, D. Zhang, L. Du, J. Hu, and Z. Liu, Impact of Reversed Austenite on the Impact Toughness of the High-Strength Steel of Low Carbon Medium Manganese, *JOM*, 2018, **70**(5), p 672–679

12. S. Yamanaka, T. Iwamoto, and T. Sawa, Study on Capturing Transformation Thermomechanical Behaviour of TRIP Steel During Impact Compression, *Mater. Res. Innov.*, 2011, **15**, p 131–134

13. K.M. Zhao, Y. Chang, P. Hu, and Y.C. Wu, Influence of Rapid Cooling Pretreatment on Microstructure and Mechanical Property of Hot Stamped AHSS Part, *J. Mater. Process. Technol.*, 2016, **228**, p 68–75

14. X.D. Li, Y. Chang, C.Y. Wang, P. Hu, and H. Dong, Comparison of the Hot-Stamped Boron-Alloyed Steel and the Warm-Stamped medium-Mn Steel on Microstructure and Mechanical Properties, *Mater. Sci. Eng., A*, 2017, **679**, p 240–248

15. Z.Q. Wu, Y.B. Tang, W. Chen, L.W. Lu, E. Li, and Z.C. Li, Exploring the Influence of Al Content on the Hot Deformation Behavior of Fe-Mn-Al-C Steels Through 3D Processing Map, *Vacuum*, 2019, **159**, p 447–455

16. Z.Y. Liang, Y.Z. Li, and M.X. Huang, The Respective Hardening Contributions of Dislocations and Twins to the Flow Stress of a Twinning-Induced Plasticity Steel, *Scr. Mater.*, 2016, **112**, p 28–31

17. J. Han, J.H. Nam, and Y.K. Lee, The Mechanism of Hydrogen Embrittlement in Intercritically Annealed Medium Mn TRIP Steel, *Acta Mater.*, 2016, **113**, p 1–10

18. H. Kamoutsi, E. Gioti, N.G. Haidemenopoulos, Z. Cai, and H. Ding, Kinetics of Solute Partitioning During Intercritical Annealing of a Medium-Mn Steel, *Mater. Trans. A*, 2015, **46A**, p 4841–4846

19. A.K. Srivastava, D. Bhattacharjee, G. Jha, N. Gope, and S.B. Singh, Microstructural and Mechanical Characterization of C-Mn-Al-Si Cold-Rolled TRIP-Aided Steel, *Mater. Sci. Eng., A*, 2007, **445-446A**, p 549–557

20. N.H.V. Dijk, A.M. Butt, L. Zhao, J. Sietsm, S.E. Offerman, J.P. Wright, and S. Zwaag, Thermal Stability of Retained Austenite in Trip Steels Studied by SYNCHROTRON X-ray Diffraction During Cooling, *Acta Mater.*, 2005, **53**, p 5439–5447

21. V.S.A. Challa, X.L. Wan, M.C. Somani, L.P. Karjalainen, and R.D.K. Misra, Significance of Interplay Between Austenite Stability and Deformation Mechanisms in Governing Three-Stage Work Hardening Behavior of Phase-Reversion Induced Nanograined/Ultrafine-Grained (NG/UFG) Stainless Steels with High Strength-High Ductility Combination, *Scr. Mater.*, 2014, **86**, p 60–63

22. Z.C. Li, X.T. Zhang, Y.J. Mou, Z.H. Cai, R.D.K. Misra, L.F. He, H.P. Li, and H. Ding, Design of an Effective Heat Treatment Involving Intercritical Hardening for High Strength-High Elongation of 0.2C-1.5Al-(6-8.5)Mn-Fe TRIP Steels: Microstructural Evolution and Deformation Behavior, *Mater. Sci. Technol.*, 2020, **36**, p 500–510

23. X.C. Wei, R.Y. Fu, and L. Li, Tensile Deformation Behavior of Cold-Rolled TRIP-Aided Steels Over Large Range of Strain Rates, *Mater. Sci. Eng., A*, 2007, **465**, p 260–266

24. R. Tian, L. Li, B.C. De Cooman, X.C. Wei, and P. Sun, Effect of Temperature and Strain Rate on Dynamic Properties of Low Silicon TRIP Steel, *J. Iron. Steel Res. Int.*, 2006, **13**, p 51–56

25. M.T. Kim, T.M. Park, K.-H. Baik, W.S. Choi, P.-P. Choi, and J. Han, Crucial Microstructural Feature to Determine the Impact Toughness of Intercritically Annealed Medium-Mn Steel with Triplex-Phase Microstructure, *Acta Mater.*, 2019, **164**, p 122–134

26. J. Han, A.K. da Silva, D. Ponge, D. Raabe, S.M. Lee, Y.-K. Lee, S.I. Lee, and B. Hwang, The Effects of Prior Austenite Grain Boundaries and Microstructural Morphology on the Impact Toughness of Intercritically Annealed Medium Mn Steel, *Acta Mater.*, 2017, **122**, p 199–206

27. M. Kuzmina, D. Ponge, and D. Raabe, Grain Boundary Segregation Engineering and Austenite Reversion Turn Embrittlement into Toughness: Example of a 9 wt% Medium Mn Steel, *Acta Mater.*, 2015, **86**, p 182–192

28. G. Lacroix, T. Pardoen, and P.J. Jacques, The Fracture Toughness of TRIP-Assisted Multiphase Steels, *Acta Mater.*, 2008, **56**, p 3900–3913

29. T. Neeraj, R. Srinivasan, and J. Li, Hydrogen Embrittlement of Ferritic Steels: Observations on Deformation Microstructure, Nanoscale Dimples and Failure by Nanovoiding, *Acta Mater.*, 2012, **60**, p 5160–5171

30. Y.J. Mou, Z.C. Li, X.T. Zhang, R.D.K. Misra, L.F. He, and H.P. Li, Design of an Effective Heat Treatment Involving Intercritical Hardening for High Strength-High Elongation of 0.2C-3Al-(6-8.5)Mn-Fe TRIP Steels: Microstructural Evolution and Deformation Behavior, *Metals*, 2019, **9**, p 1275–1284

31. A. Das and S. Tarafder, Geometry of Dimples and its Correlation with Mechanical Properties in Austenitic Stainless Steel, *Scr. Mater.*, 2008, **59**, p 1014–1017

Publisher's Note Springer Nature remains neutral with regard to jurisdictional claims in published maps and institutional affiliations.